# A boundary-volume integral equation method for the analysis of wave scattering

Terumi Touhei*

*Department of Civil Engineering, Tokyo University of Science, 2641 Yamazaki, Noda City 278-8510, Japan*

**Abstract.** A method for the analysis of wave scattering in 3-D elastic full space is developed by means of the coupled boundary-volume integral equation, which takes into account the effects of both the boundary of inclusions and the uctuation of the wave field. The wavenumber domain formulation is used to construct the Krylov subspace by means of FFT. In order to achieve the wavenumber domain formulation, the boundary-volume integral equation is transformed into the volume integral equation. The formulation is also focused on this transform and its numerical implementation. Several numerical results clarify the accuracy and effectiveness of the present method for scattering analysis.

**Keywords:** coupled boundary-volume integral equation; fast Fourier transform; elastic wave scattering; wavenumber domain formulation; Krylov subspace iteration technique

## 1. Introduction

Since the 1980s, the integral equation method has been important for the analysis of wave scattering. The integral equation obtained by means of Green's function is a direct representation of the solution of the wave field satisfying the radiation condition, which leads to straightforward numerical methods based on linear algebra. A number of studies in the field of scattering analysis have used the integral equation. For example, Colton and Kress (1983,1998) presented methods for acoustic and electromagnetic wave propagation based on the theory of operators and reported a survey of a number of articles on the forward and inverse scattering analysis, Guzina *et al* (2003) considered the problem of mapping underground cavities from surface seismic measurements based on a regularized boundary integral equation, and Manolis *et al.* (2004) dealt with elastic wave scattering due to cracks in inhomogeneous geological continua by introducing the boundary integral equation. Moreover, a number of studies have been based on the volume integral equation, which is based on the Lippmann-Schwinger equation (Ikebe 1960). Yang *et al.* (2008) proposed a conjugate gradient fast Fourier transform (CG-FFT) approach to solve elastic scattering problems, and De Zaeytijd *et al.* (2008) proposed a fast Fourier transform and high-frequency multilevel fast multipole algorithm (MLFMA-FFT) for analyzing electromagnetic waves.

The present author also presented a volume integral equation method based on the wavenumber

---

domain formulation (Touhei 2009, Touhei *et al*. 2009 and Touhei 2011). This method used the Fourier transform to construct the Krylov subspace (Barrett *et al*. 1994) according to the mathematical form of the volume integral equation in the wavenumber domain. As a result, it was not necessary to calculate a coefficient matrix for the integral equation. Furthermore, the development of a fast method was possible by developing a fast algorithm, even for the case of an elastic half space. However, for simplicity, the volume integral equation method generally excludes the boundary terms that cause scattered waves. Nevertheless, for the analysis of scattered elastic waves, it is desirable to be able to take into account the effects of both boundaries and uctuations of the wave field.

Under the above-described circumstances, the goal of the present study is to establish an integral equation method that incorporates the effects of the boundaries as well as the uctuation of the wave field. The staring point of the formulation is the representation of the 3-D elastic wave field by means of the coupled boundary-volume integral equation.

The method for the integral equation is an extension of the method presented in a previous paper (Touhei 2009). In order to apply the Fourier transform to the coupled boundary-volume integral equation, the equation is transformed into a volume integral equation, which is an important task during the formulation. Numerical calculations are carried out in order to verify the above formulations as well as to examine the convergence properties of the solution. The discussion of the present paper begins with the presentation of the coupled boundary-volume integral equation.

## 2 Formulation of the coupled boundary and volume integral equation method

### 2.1 Definition of the problem and basic notation

Fig. 1 shows the concept of the scattering problem defined in this article. An incident wave in a 3-D elastic full space is propagating toward inhomogeneous region. The inhomogeneous region is made up of fluctuating areas and inclusions that can be characterized by cavity or rigid boundary conditions. The problem is to determine the scattered wave field by means of the coupled boundary-volume integral equation method that is developed in the present study based on the wavenumber domain formulation.

This section denes the problem and basic notation used to prepare the formulation of the present method.

According to Fig. 1, let 3-D elastic full space be divided into the following

$$\mathbb{R}^3 = \Omega_e \cup \Omega_i \cup \Gamma \tag{1}$$

where $\Omega_i$ is the region of the inclusions, $\Gamma$ is the boundary of the inclusions, and $\Omega_e$ is the region outside the inclusions. Note that the fluctuating areas are included in $\Omega_e$. A Cartesian coordinate system is used for the wave field. The spatial point in the wave field is expressed as

$$x = (x_j) = (x_1,\, x_2,\, x_3) \in \mathbb{R}^3 \tag{2}$$

where the subscript index indicates the component of the vector. The fluctuating areas are expressed by the deviation of the Lamé constants from the background constants as follows
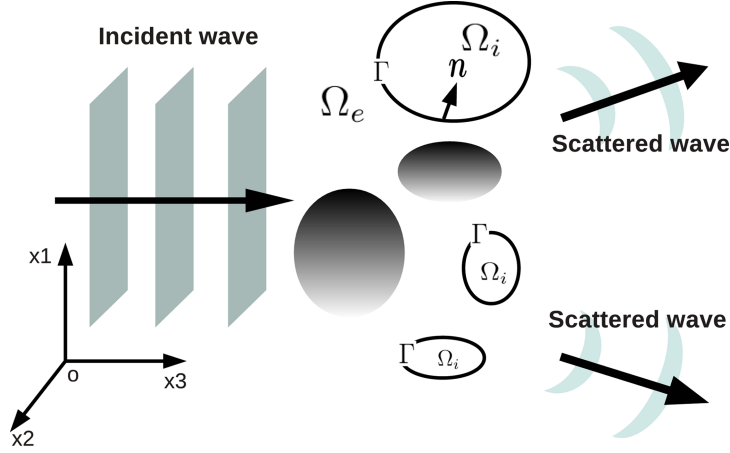
Fig. 1 Concept of the analyzed model

$$\lambda(x) = \lambda_0 + \tilde{\lambda}(x)$$

$$\mu(x) = \mu_0 + \tilde{\mu}(x) \tag{3}$$

where $\lambda_0$ and $\mu_0$ are the background Lamé constants of the wave field, and $\tilde{\lambda}$ and $\tilde{\mu}$ are their fluctuations. The support of the functions describing the fluctuation of the wave field, $\tilde{\lambda}$ and $\tilde{\mu}$, must be in $\Omega_e$, i.e.

$$\text{supp } \tilde{\lambda}(x) \subset \Omega_e, \qquad \text{supp } \tilde{\mu}(x) \subset \Omega_e \tag{4}$$

The time factor of the wave field in this article is assumed to be $exp(-i\omega t)$ where $\omega$ is the circular frequency, and $t$ is the time. Then, the equilibrium equation of the wave field is expressed as

$$\partial_j \sigma_{ij}(x) + \rho \omega^2 u_i(x) = 0 \tag{5}$$

where $\sigma_{ij}$ is the stress tensor defined at the point $x$, $\partial_j$ is the partial differential operator, $\rho$ is the mass density, and $u_i$ is the displacement field. The subscript indexes $i$ and $j$ in Eq. (5) are the components of the Cartesian coordinate system to which the summation convention is applied. The constitutive equation showing the relationship between the stress and strain tensors is as follows

$$\sigma_{ij} = \lambda \delta_{ij} \varepsilon_{kk} + 2\mu \varepsilon_{ij} \tag{6}$$

where $\delta_{ij}$ is the Kronecker delta, and $\varepsilon_{ij}$ is the strain tensor given by

$$\varepsilon_{ij} = (1/2)(\partial_i u_j + \partial_j u_i) \tag{7}$$

The boundary conditions at the boundary of the inclusions are

$$\sigma_{ij}(x)n_j(x) = 0, \qquad x \in \Gamma_1 \tag{8}$$

for the free traction condition and

$$u_i(x) = 0, \qquad x \in \Gamma_2 \tag{9}$$

for the rigid boundary condition, where

$$\Gamma = \Gamma_1 \cup \Gamma_2, \quad \Gamma_1 \cap \Gamma_2 = \phi \tag{10}$$

and $n_i$ is the component of the normal vector at the boundary for which the direction is inward to the inclusions.

### 2.2 Coupled boundary-volume integral equation in the space domain

Substituting Eqs. (7) and (6) into Eq. (5) yields the following governing equation for the present problem

$$(L_{ij}(\partial) + \delta_{ij}\rho\omega^2)u_j(x) = N_{ij}(\partial, x)u_j(x) \tag{11}$$

where $L_{ij}(\partial)$ and $N_{ij}(\partial, x)$ are the differential operators constructed by the background Lamé constants and their fluctuations, respectively. The explicit forms of the operators $L_{ij}$ and $N_{ij}$ are given by

$$L_{ij}(\partial) = (\lambda_0 + \mu_0)\partial_i\partial_j + \mu_0\delta_{ij}\partial_k\partial_k \tag{12}$$

$$N_{ij}(\partial, x) = -(\tilde{\lambda}(x) + \tilde{\mu}(x))\partial_i\partial_j - \delta_{ij}\tilde{\mu}(x)\partial_k\partial_k$$
$$-\partial_i\tilde{\lambda}(x)\partial_j - \delta_{ij}\partial_k\tilde{\mu}(x)\partial_k - \partial_j\tilde{\mu}(x)\partial_i \tag{13}$$

The boundary-volume integral equation can now be presented. Assume that the righthand side of Eq. (11) is the inhomogeneous term for the equation. Based on the representation theorem (Aki and Richards 2002) and literature of the boundary method (for example, Brebbia and Walker 1980), the solution of Eq. (11) is expressed by the following integral equation

$$c_{ij}(x)u_j(x) = u_i^{(I)}(x) - \int_{\mathbb{R}^3} G_{ij}(x, y)N_{jk}(\partial, y)u_k(y)dy$$

$$+ \int_\Gamma (G_{ij}(x, y)\sigma_{jk}(y)n_k(y) - T_{ij}(x, y)u_j(y))d\Gamma$$

$$(x \in \Omega_e \cup \Gamma \cup \Omega_i = \mathbb{R}^3) \tag{14}$$

where $u_i^{(I)}$ is the incident wave, $G_{ij}$ is the Green's function, $T_{ij}$ is the Green's function describing the traction, and $c_{ij}(x)$ is the function defined by

$$c_{ij}(x) = \begin{cases} \delta_{ij} & x \in \Omega_e \\ (1/2)\delta_{ij} & x \in \Gamma \\ 0 & x \in \Omega_i \end{cases} \tag{15}$$

for the case in which the boundaries are smooth. The Green's function $G_{ij}$ is defined as follows

$$(L_{ij}(\partial) + \delta_{ij}\rho\omega^2)G_{jk}(x,y) = -\delta_{ik}\delta(x-y), \quad x,y \in \mathbb{R}^3 \tag{16}$$

where $\delta_{ij}$ is the Kronecker delta, and $\delta(\cdot)$ is the Dirac delta function. The explicit form of the Green's function is expressed as

$$G_{ij}(x,y) = \frac{\delta_{ij}}{4\pi\mu_0 r}exp(ik_T r) + \frac{1}{4\pi\mu_0 k_T^2}\partial_i\partial_j\left[\frac{exp(ik_T r) - exp(ik_L r)}{r}\right] \tag{17}$$

where $r = |x-y|$ and $k_T$ and $k_L$ are the wavenumber for the $S$ and $P$ waves, respectively, defined by

$$k_T = \frac{\omega}{\sqrt{\mu_0/\rho}}, \quad k_L = \frac{\omega}{\sqrt{(\lambda_0 + 2\mu_0)/\rho}} \tag{18}$$

The Green's function for the traction is derived from $G_{ij}$, such that

$$T_{ij}(x,y) = (M_{jkl}(\partial_y)G_{il}(x,y))n_k(y) \tag{19}$$

where $M_{ijk}(\partial)$ is the operator

$$M_{ijk}(\partial) = \lambda_0\delta_{ij}\partial_k + \mu_0\delta_{jk}\partial_i + \mu_0\delta_{ik}\partial_j \tag{20}$$

and $\partial_y$ indicates that this partial differential operator is for the coordinate $y$.

### 2.3 Transform of the boundary integral to the volume integral

In order to achieve the wavenumber domain formulation for the integral equation, Eq. (14) must be transformed into the volume integral equation. For this purpose, we introduce the function $\delta_\Gamma$, which has the following properties

$$\int_{\mathbb{R}^3}\delta_\Gamma(y)u(y)dy = \int_\Gamma u(y)d\Gamma_y \tag{21}$$

For the construction of $\delta_\Gamma$, take a point $x^{(\Gamma)}$ in $\Gamma$, and let $U$ be the neighborhood of $x^{(\Gamma)}$, as shown in Fig. 2. Assume that a function $\phi(x)$ having the properties

$$|\nabla\phi(x)|^2 \neq 0, \qquad (x \in U) \tag{22}$$
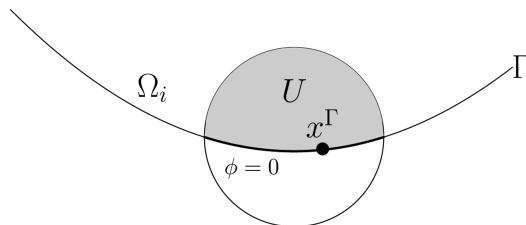


Fig. 2 Construction of $\delta_\Gamma$

*Terumi Touhei*

characterizes $\Gamma$ and $\Omega_i$ in $U$ such that

$$\Gamma \cap U = \{x \in U \mid \phi(x) = 0\}$$
$$\Omega_i \cap U = \{x \in U \mid \phi(x) > 0\} \tag{23}$$

where

$$|\nabla \phi(x)|^2 = |\partial_1 \phi(x)|^2 + |\partial_2 \phi(x)|^2 + |\partial_3 \phi(x)|^2 \tag{24}$$

Then, $\delta_\Gamma$ can be defined in $U$ by

$$\psi(x) = \frac{\phi(x)}{|\nabla \phi(x)|}, \qquad (x \in U) \tag{25}$$

as follows

$$\delta_\Gamma(x) = \delta(\psi(x)), \qquad (x \in U) \tag{26}$$

where $\delta(\cdot)$ is the 1-D Dirac delta function. Based on $\delta(\psi(x))$, we have

$$\int_U \delta_\Gamma(x) u(x) dx = \int_{\Gamma \cap U} u(x) d\Gamma_x \tag{27}$$

In order to obtain $\delta_\Gamma$ in $\mathbb{R}^3$, let $\Gamma$ be covered by $\{U\}_{j=1}^n$, such that

$$\Gamma \subset \bigcup_{j=1}^n U_j$$
$$U_j \cap U_i = \phi, \quad i \neq j \tag{28}$$

and $\psi_j(x)$ let be the function satisfying Eq. (27) for each $U_j$. Then, $\delta_\Gamma$ in $\mathbb{R}^3$ is expressed as

$$\delta_\Gamma(x) = \sum_{j=1}^n \chi_{U_j}(x) \delta(\psi_j(x)) \tag{29}$$
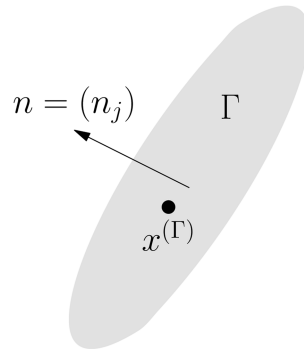


Fig. 3 Sample of the construction of $\delta_\Gamma$

where $\chi_U$ is the definition function defined by

$$\chi_U(x) = \begin{cases} 1 & x \in U \\ 0 & x \notin U \end{cases} \tag{30}$$

As a simple example for Eq. (26), consider the boundary $\Gamma$ as a plane shown in Fig. 3. Let the equation of the plane be

$$\psi(x) = n_j(x_j - x_j^{(\Gamma)}) = 0, \quad x^{(\Gamma)} = (x_j^{(\Gamma)}) \in \Gamma \tag{31}$$

where $n_j$, ($j = 1,2,3$) is the normal vector of the plane. Then, $\delta_\Gamma$ for the plane becomes

$$\delta_\Gamma(x) = \chi_\Gamma(x)\delta(n_j(x_j - x_j^{(\Gamma)})) \tag{32}$$

Next, by means of $\delta_\Gamma$, Eq. (14) is transformed into a volume integral equation as follows:

$$u_i(x) = u_i^{(I)}(x) - \int_{\mathbb{R}^3} G_{ij}(x, y) N_{jk}(\partial_y, y) \upsilon_k(y) dy$$

$$+ \int_{\mathbb{R}^3} \delta_\Gamma(y) [G_{ij}(x, y)(M_{jkl}(\partial_y)\upsilon_k(y))n_l(y)$$

$$-(M_{jkl}(\partial_y) G_{il}(x, y))n_k(y)\upsilon_j(y)] dy, \quad (x \in \Omega_e \cup \Omega_i) \tag{33}$$

where $v_i(y)$ is defined by

$$\upsilon_i(y) = \begin{cases} u_i(y) & \text{when } y \in \Omega_e \cup \Gamma \\ 0 & \text{when } y \in \Omega_i \end{cases} \tag{34}$$

Eq. (14) is constructed for $x \in \Omega_e \cup \Omega_i$ and $x \notin \Gamma$ to avoid the singular integral related to the Green's function for the traction. In addition, we assumed that the boundary value of the displacement and traction at $\Gamma$ is obtained from the limit of displacement and the stress field in $\Omega_e$, namely

$$\upsilon_j(x)\big|_\Gamma = \lim_{x \in \Omega_e \to \Gamma} u_j(x)$$

$$M_{jkl}(\partial)\upsilon_k(x)\big|_\Gamma = \lim_{x \in \Omega_e \to \Gamma} M_{jkl}(\partial)u_k(x) \tag{35}$$

where the left-hand side of the above equation denotes the boundary values.

It is true that the transform of the boundary-volume integral equation into the volume integral equation may be also possible not by $\delta_\Gamma$ but by means of the Gauss divergence theorem. The use of the Gauss divergence theorem, however, requires the complicated formulation. For example, we have to obtain the derivative of functions such as $M_{jkl}(\partial_y)$ $G_{il}(x,y)$ shown in Eq. (19). In this sense, the use of $\delta_\Gamma$ simplifies the formulation. In addition, the similarity of the use of $\delta_\Gamma$ and the Radon transform should be also mentioned here.

According to the definition of the Radon transform (for example, Markoe 2006), the right side of Eq. (21) is the Radon transform in $\mathbb{R}^3$ itself, in the case that $\Gamma$ is a plane in $\mathbb{R}^3$. Due to the introduction of $\delta_\Gamma$, however, it becomes possible that $\Gamma$ has a curvature. Therefore, Eq. (21) can be

assumed to be an extension of the Radon transform.

### 2.4 Fourier transform and its application to the integral equation

The expressions for the Fourier transform and its inverse transform used in the present study are as follows

$$
\begin{aligned}
(\mathscr{F}u_i)(\xi) &= \int_{\mathbb{R}^3} u_i(x)\varphi^*(\xi, x)dx \\
(\mathscr{F}^{-1}\hat{u}_i)(x) &= \int_{\mathbb{R}^3} \hat{u}_i(\xi)\varphi(\xi, x)d\xi
\end{aligned}
\tag{36}
$$

where $\xi$ is the point in the wavenumber space, the components of which are expressed as

$$
\xi = (\xi_j) = (\xi_1, \xi_2, \xi_3) \in \mathbb{R}^3
\tag{37}
$$

$\varphi(\xi, x)$ are the kernel of the transforms defined as

$$
\varphi(\xi, x) = \frac{1}{\sqrt{2\pi}^3} exp(i(x_1\xi_1 + x_2\xi_2 + x_3\xi_3))
\tag{38}
$$

and $\varphi^*$ is the complex conjugate of $\varphi$. Note that $\mathscr{F}$ and $\mathscr{F}^{-1}$ are the operators for the Fourier transform and its inverse transform, respectively, and the symbol $\hat{\ }$ attached to a function is used to express the Fourier transform of the function.

The expression of the Dirac delta function for $x, y \in \mathbb{R}^3$ in terms of $\varphi(\xi, x)$ is

$$
\delta(x - y) = \int_{\mathbb{R}^3} \varphi(\xi, x)\varphi^*(\xi, y)d\xi
\tag{39}
$$

The expression of the Green's function defined by Eq. (16) is also possible in terms of $\varphi(\xi, x)$. The Fourier transform of Eq. (16) becomes

$$
(L_{ij}(i\xi) + \delta_{ij}\rho\omega^2)\hat{G}(\xi, y) = -\delta_{ik}\varphi^*(\xi, y)
\tag{40}
$$

where $L_{ij}(i\xi)$ is obtained from Eq. (12) by substituting $i\xi_j$ into $\partial_j$. The solution of Eq. (40) becomes

$$
\hat{G}_{ij}(\xi, y) = \hat{h}_{ij}(\xi)\varphi^*(\xi, y)
\tag{41}
$$

where $\hat{h}_{ij}$ is defined by

$$
(L_{ij}(i\xi) + \delta_{ij}\rho\omega^2)\hat{h}_{ij}(\xi) = -\delta_{ik}
\tag{42}
$$

Therefore, by means of $\hat{h}_{ij}$, the Green's function in terms of $\varphi(\xi, x)$ is given as

$$
G_{ij}(x, y) = \int_{\mathbb{R}^3} \varphi(\xi, x)\hat{h}_{ij}(\xi)\varphi^*(\xi, y)d\xi
\tag{43}
$$

Note that the explicit form of $\hat{h}_{ij}$ is

$$\hat{h}_{ij}(\xi) = \frac{1}{\mu_0} \frac{\delta_{ij}}{\xi^2 - k_T^2 - i\varepsilon}$$

$$-\frac{1}{2\mu_0(1-\nu)} \frac{\xi_i \xi_j}{(\xi^2 - k_T^2 - i\varepsilon)(\xi^2 - k_L^2 - i\varepsilon)} \tag{44}$$

where $\varepsilon$ is an infinitesimally small positive number, $\nu$ is the Poisson ratio, and

$$\xi^2 = \xi_1^2 + \xi_2^2 + \xi_3^2 \tag{45}$$

As expected, the result of evaluating the integral of Eq. (43) agrees with Eq. (17).

Function $\hat{h}_{ij}(\xi)$ is important with respect to the Fourier transform for the integral equation. For example, let us define the following equation

$$u_i(x) = \int_{\mathbb{R}^3} G_{ij}(x, y) f_i(y) dy \tag{46}$$

The process of the Fourier transform for $u_i$ becomes

$$\hat{u}_i(\xi) = \int_{\mathbb{R}^3} \varphi^*(\xi, x) \int_{\mathbb{R}^3} G_{ij}(x, y) f_j(y) dy dx$$

$$= \hat{h}_{ij}(\xi) \int_{\mathbb{R}^3} \varphi^*(\xi, y) f_j(y) dy = \hat{h}_{ij}(\xi) \hat{f}_j(\xi) \tag{47}$$

Namely, the Fourier transform of $\hat{u}_i(\xi)$ can be decomposed into the product of $\hat{h}_{ij}$ and $\hat{f}_j$, that is according to the fact that Eq. (46) is the convolution integral.

Similar results can also be found in the stress field due to the Green's function

$$S_{ijk}(x, y) = M_{jkl}(\partial_y) G_{ijl}(x, y) \tag{48}$$

The stress field in terms of $\varphi(\xi, x)$ is given by

$$S_{ijk}(x, y) = \int_{\mathbb{R}^3} \varphi(\xi, x) \hat{\sigma}_{ijk}(\xi) \varphi^*(\xi, y) d\xi \tag{49}$$

where $\hat{\sigma}_{ijk}$ is given as

$$\hat{\sigma}_{ijk}(\xi) = M_{jkl}(-i\xi) \hat{h}_{ij}(\xi) \tag{50}$$

Therefore, the Fourier transform of the following function

$$u_i(x) = \int_{\mathbb{R}^3} S_{ijk}(x, y) f_{jk}(y) dy \tag{51}$$

becomes

$$\hat{u}_i(\xi) = \hat{\sigma}_{ijk}(\xi) \hat{f}_{jk}(\xi) \tag{52}$$

Next, based on Eqs. (47) and (52), the application of the Fourier transforms to Eq. (14) becomes

possible. The application of the Fourier transform to Eq. (33) yields

$$\hat{\upsilon}_i(\xi) = \hat{f}_i(\xi) - \mathscr{A}_{ij}\hat{\upsilon}_j(\xi), \quad \xi \in \mathbb{R}^3 \tag{53}$$

where $\mathscr{A}_{ij}$ is the operator defined by

$$\begin{aligned}
\mathscr{A}_{ij} &= \hat{h}_{ik}(\xi)\mathscr{F}N_{kj}\mathscr{F}^{-1} \\
&+ \hat{h}_{ik}(\xi)\mathscr{F}\delta_\Gamma M_{kjl}n_l\mathscr{F}^{-1} \\
&- \hat{\sigma}_{ikj}(\xi)\,\mathscr{F}\delta_\Gamma n_k\mathscr{F}^{-1}
\end{aligned} \tag{54}$$

Eq. (53) is the boundary-volume integral equation in the wavenumber domain. The operator given in Eq. (54) involves the Fourier transform and its inverse transform rather that the integral operators in the space domain. The remainder of the present paper investigates the discretization of the equation and the verification of the possibility of solving the equation based on the Krylov subspace method and FFT.

## 2.5 Discretization method for the integral equation

Let us define the set of the finite number of grid points in $\mathbb{R}^3$

$$\begin{aligned}
D_x &= \{(n_1\Delta x_1, n_2\Delta x_2, n_3\Delta x_3) \mid n_1 \in \mathbb{N}_1, n_2 \in \mathbb{N}_2, n_3 \in \mathbb{N}_3\} \subset \mathbb{R}^3 \\
D_\xi &= \{(n_1\Delta\xi_1, n_2\Delta\xi_2, n_3\Delta\xi_3) \mid n_1 \in \mathbb{N}_1, n_2 \in \mathbb{N}_2, n_3 \in \mathbb{N}_3\} \subset \mathbb{R}^3
\end{aligned} \tag{55}$$

to discretize Eq. (53), where $\Delta x_j$, $(j = 1,2,3)$ is the interval of the grid points in the space domain, $\Delta\xi_j$, $(j = 1,2,3)$ is the interval of the grid points in the wavenumber domain, and $\mathbb{N}_1$, $\mathbb{N}_2$, and $\mathbb{N}_3$ are the sets of integers defined by

$$\begin{aligned}
\mathbb{N}_1 &= \{n \mid -N_1/2 \le n < N_1/2\} \\
\mathbb{N}_2 &= \{n \mid -N_2/2 \le n < N_2/2\} \\
\mathbb{N}_3 &= \{n \mid -N_3/2 \le n < N_3/2\}
\end{aligned} \tag{56}$$

Note that $(N_1, N_2, N_3)$ defines the number of grid points in $\mathbb{R}^3$.

The discrete Fourier transform is defined on the set of the grid points $D_x$ and $D_\xi$, such that

$$\begin{aligned}
(\mathscr{F}_D f_i)(\xi^{(p)}) &= \frac{\Delta x}{\sqrt{2\pi}^3} \sum_{q \in \mathbb{N}_1 \times \mathbb{N}_2 \times \mathbb{N}_3} f_i(x^{(q)})exp(-ix^{(q)} \cdot \xi^{(p)}) \\
(\mathscr{F}_D^{-1}\hat{f}_i)(x^{(q)}) &= \frac{\Delta\xi}{\sqrt{2\pi}^3} \sum_{p \in \mathbb{N}_1 \times \mathbb{N}_2 \times \mathbb{N}_3} \hat{f}_i(\xi^{(p)})exp(ix^{(q)} \cdot \xi^{(p)})
\end{aligned} \tag{57}$$

where $\mathscr{F}_D$ and $\mathscr{F}_D^{-1}$ are the operators for the discrete Fourier and its inverse transforms, $\Delta x$ and $\Delta\xi$ are defined by

$$\Delta x = \Delta x_1\Delta x_2\Delta x_3, \quad \Delta\xi = \Delta\xi_1\Delta\xi_2\Delta\xi_3 \tag{58}$$

and $x^{(q)}$ and $\xi^{(p)}$ are the grid point in the space and wavenumber domain that can be expressed by

$$x^{(p)} = (x_1^{(p_1)}, x_2^{(p_2)}, x_3^{(p_3)}) \tag{59}$$

$$\xi^{(q)} = (\xi_1^{(q_1)}, \xi_2^{(q_2)}, \xi_3^{(q_3)}) \tag{60}$$

In Eq. (60), note that

$$x_j^{(p_j)} = \Delta x_j p_j, \quad \xi_j^{(q_j)} = \Delta \xi_j q_j, \quad (j = 1, 2, 3) \tag{61}$$

There is a relationship between $\Delta x_j$ and $\Delta \xi_j$ such that

$$\Delta x_j \Delta \xi_j = \frac{2\pi}{N_j}, \quad (j = 1, 2, 3) \tag{62}$$

It is necessary to clarify the treatment of the derivative of the functions, as well as the Dirac delta function, in the application of the discrete Fourier transform. The calculation of the derivative of a function by means of the discrete Fourier transform is not very difficult. For example, $\partial_i f(x)$ in terms of the discrete Fourier transform is expressed by

$$\partial_i f(x) = (\mathscr{F}_D^{-1}(i\xi_i \mathscr{F}_D f))(x), \quad x \in D_x, \xi \in D_\xi \tag{63}$$

On the other hand, the treatment for the Dirac delta function in the discrete Fourier transform is not self-evident. In order to resolve this problem, recall the delta function represented by the Fourier series, which is as follows

$$\delta(x_j - y_j) = \frac{1}{L} \sum_{p=-\infty}^{\infty} exp\left[\frac{2\pi i}{L} p(x_j - y_j)\right], \quad x_j, y_j \in \mathbb{R} \tag{64}$$

where $L$ is a positive constant that describes the period of the Dirac delta function. Next, we reduce the infinite series of Eq. (64) to a finite sum. The function expressed by this finite series should be used as the delta function in the discrete Fourier transform. We express this function as follows

$$\tilde{\delta}(x_j - y_j) = \frac{1}{L} \sum_{p=-N_j/2}^{N_j/2-1} exp\left[\frac{2\pi i}{L} p(x_j - y_j)\right], \quad x_j, y_j \in \mathbb{R} \tag{65}$$

Next, we set

$$L = N_j \Delta x_j, \quad x_j = n\Delta x_j, \quad y_j = m\Delta x_j \tag{66}$$

Then, Eq. (65) becomes

$$\tilde{\delta}(x_j - y_j) = \frac{1}{N_j \Delta xj} \sum_{p=-N_j/2}^{N_j/2-1} exp\left[\frac{2\pi i}{N_j \Delta x_j} p(n-m)\Delta x_j\right]$$

$$= \frac{S_{nm}}{\Delta \alpha_j} \tag{67}$$

According to Eq. (65), $\tilde{\delta}$ has several important properties. Let the discrete Fourier transform of $\tilde{\delta}(x_j - y_j)$ be expressed by $\hat{\tilde{\delta}}(\xi_j)$. Then, $\hat{\tilde{\delta}}(\xi_j)$ becomes

$$\hat{\tilde{\delta}}(\xi_j) = \frac{\Delta x_j}{\sqrt{2\pi}} \sum_{n=-N_j/2}^{N_j/2-1} \frac{\delta_{nm}}{\Delta x_j} exp\left[-\frac{2\pi i}{N_j}kn\right]$$

$$= \frac{1}{\sqrt{2\pi}} exp\left(-\frac{2\pi i}{N_j}km\right) \tag{68}$$

which agrees with the following result

$$\hat{\delta}(\xi_j) = \frac{1}{\sqrt{2\pi}}\int_{-\infty}^{+\infty} \delta(x_j - y_j) exp(-ix_j\xi_j)dx_j$$

$$= \frac{1}{\sqrt{2\pi}} exp(-i\xi_j y_j) \tag{69}$$

This agreement can be clarified by setting $\xi_j = k\Delta\xi_j$ and $y_j = m\Delta x_j$. Furthermore, $\tilde{\delta}$ has the following property

$$f_m = \sum_{n=-N_j/2}^{N_j/2-1} \frac{\delta_{nm}}{\Delta x_j}f_n\Delta x_j \tag{70}$$

which corresponds to

$$f(y_j) = \int_{-\infty}^{\infty} \delta(x_j - y_j)f(x_j)dx_j \tag{71}$$

Eqs. (68) and (70) are found to be desirable properties as the delta function in the process of the discrete Fourier transform. Therefore, we use $\tilde{\delta}$ for the delta function to construct $\delta_\Gamma$ shown in Eq. (29) in the numerical calculations.

The Krylov subspace method (Barrett *et al.* 1994) can be applied to Eq. (53) after the equation is discretized. In the process of discretizing the equation, note that the function $\upsilon_i$ to be obtained from Eq. (53) was discontinuous at the boundary $\Gamma$, as shown in Eq. (34). The convergence of the Fourier series at the discontinuous point is to its average. Namely, the solution of the discretized equation for Eq. (53) at the $\Gamma$ is

$$\upsilon_j(x)|_\Gamma = (1/2)(\lim_{x\in\Omega_e\to\Gamma}\upsilon_j(x) + \lim_{x\in\Omega_i\to\Gamma}\upsilon_j(x))$$

$$= (1/2)\lim_{x\in\Omega_e\to\Gamma}\upsilon_j(x) \tag{72}$$

which is different from Eq. (35). In order to resolve this problem, the discretized equation for Eq. (53) should be expressed by

$$\hat{\upsilon}_i(\xi) = \hat{f}_i(\xi) - \mathscr{A}_{Dij}\hat{\upsilon}_j(\xi), \quad \xi \in D_\xi \subset \mathbb{R}^3 \tag{73}$$

where $\mathscr{A}_{Dij}$ is the discretized operator, such that

$$\mathscr{A}_{Dij} = \hat{h}_{ik}(\xi)\,\mathscr{F}_D\,N_{kj}(\partial,x)\,\mathscr{F}_D^{-1}$$
$$+ \hat{h}_{ik}(\xi)\,\mathscr{F}_D\,(2\tilde{\delta}_\Gamma(x))M_{kjl}(\partial)n_l(x)\,\mathscr{F}_D^{-1}$$
$$-\hat{\sigma}_{ikj}(\xi)\,\mathscr{F}_D\,(2\tilde{\delta}_\Gamma(x))n_k(x)\,\mathscr{F}_D^{-1}, \quad x \in D_x, \ \xi \in D_\xi \qquad (74)$$

Note that $\tilde{\delta}_\Gamma$ is constructed by $\tilde{\delta}$ defined in Eq. (67). As can be seen in Eq. (74), the effects of the boundary terms must be taken into account by $2\tilde{\delta}_\Gamma$ due to Eq. (72). The effectiveness of the representation of the operator shown in Eq. (74) is verified in the numerical examples presented below.

## 3. Numerical examples

### 3.1 Scattering analysis due to a rigid inclusion

As the first numerical example, let us examine the scattering analysis due to a rigid inclusion embedded in a homogeneous elastic wave field. The analysis involves solving Eq. (73) for the operator

$$\mathscr{A}_{Dij} = \hat{h}_{ik}(\xi)\,\mathscr{F}_D\,(2\tilde{\delta}_\Gamma(x))M_{kjl}(\partial)n_l(x)\,\mathscr{F}_D^{-1} \qquad (75)$$

For the homogeneous wave field, the $P$ and $S$ wave velocities are set to 2 km/s and 1 km/s, respectively, the mass density is 2 g/cm$^3$, and the frequency is 1 Hz. Therefore, the wavelengths of the $P$ and $S$ waves become 2 km and 1 km, respectively. The incident wave in the wave field is the $P$ wave propagating in the $x_3$ direction. The $P$ wave potential for the incident wave is given as

$$\Phi(x) = A\,exp(ik_L x_3) \qquad (76)$$

where $A$ is the amplitude of the potential, which is taken as $A = 1.0 \times 10^5$ cm$^2$ for the numerical calculation. The incident wave field based on the $P$ wave potential is given as

$$u_i^{(I)}(x) = \partial_i A\,exp(ik_L x_3) \qquad (77)$$

In order to discretize the wave field for the present integral equation method, the number of grid points are set by $N_1 = N_2 = N_3 = 256$, and the interval of the grids in the space domain is $\Delta x_1 = \Delta x_2 = \Delta x_3 = 0.25$ km, which is 1/4 of the $S$ wave length. Namely, grid points for the the present integral equation method are distributed uniformly in the range of $-32$ km $\leq x_j < 32$ km, $(j = 1,2,3)$ in the space domain.

The inclusion is a rectangular rigid solid. The area for the inclusion is

$$-1 \leq x_1/\lambda_T \leq +1, \quad -1 \leq x_2/\lambda_T \leq +1, \quad -0.5 \leq x_3/\lambda_T \leq 0.5 \qquad (78)$$

where $\lambda_T$ is the wavelength of the $S$ wave. For comparison, boundary element analysis is also carried out. The boundary element mesh for the inclusion is shown in Fig. 4, in that the number of
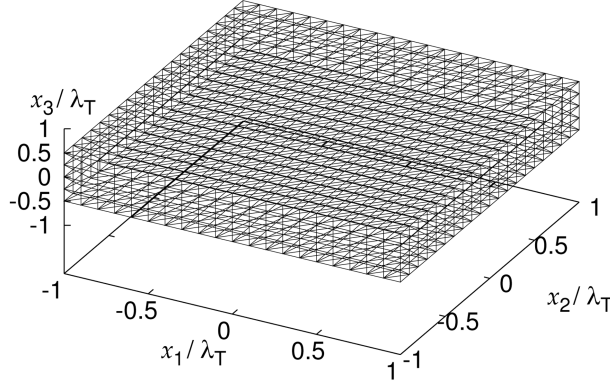
Fig. 4 Discretization of the surface $\Gamma$
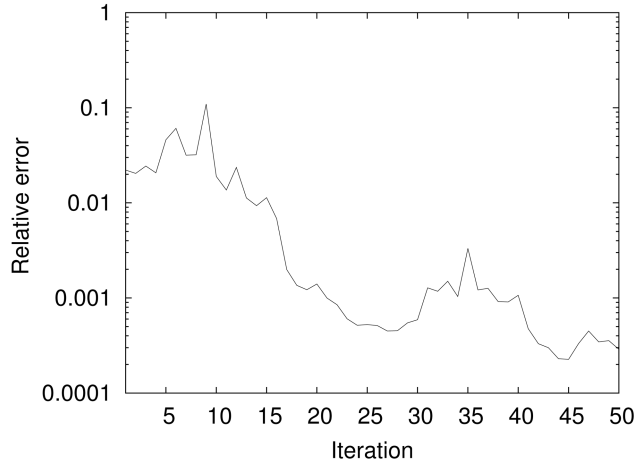


Fig. 5 Convergence properties of the solution

boundary elements is 2240 and that of the grid points is 1134.

The Bi-CGSTAB method is used to solve Eq. (73) by the iterative procedure. The convergence of the solution of Eq. (73) with respect to the number of iterations is shown in Fig. 5. The relative error $\varepsilon_r$ during the iteration is defined as

$$\varepsilon_r = \frac{\left\| \hat{\upsilon}_i(\xi) + \mathscr{A}_{Dij}\hat{\upsilon}_j(\xi) - \hat{u}_i^{(I)}(\xi) \right\|}{\left\| \hat{u}_i^{(I)}(\xi) \right\|} \tag{79}$$

where $\|\cdot\|$ is the norm of the function given as, for example

$$\left\| \hat{f}_i(\xi) \right\|^2 = \sum_{p \in \mathbb{N}_1 \times \mathbb{N}_2 \times \mathbb{N}_3} [\left| \hat{f}_1(\xi^{(p)}) \right|^2 + \left| \hat{f}_2(\xi^{(p)}) \right|^2 + \left| \hat{f}_3(\xi^{(p)}) \right|^2] \tag{80}$$

According to the convergence properties of the solution shown in Fig. 5, no decrease in the relative error is observed at the beginning of the iterative process. The relative error begins to decrease at around ten iterations. The decrease in the relative error, however, is not monotonous, and the rate of the decrease is found to slow as the number of iterations increases.

(a) $x_3/\lambda_T = 1$          (b) $x_3/\lambda_T = 3$



(c) $x_3/\lambda_T = 5$

Fig. 6 Comparison of displacement along the $x_1$ axis
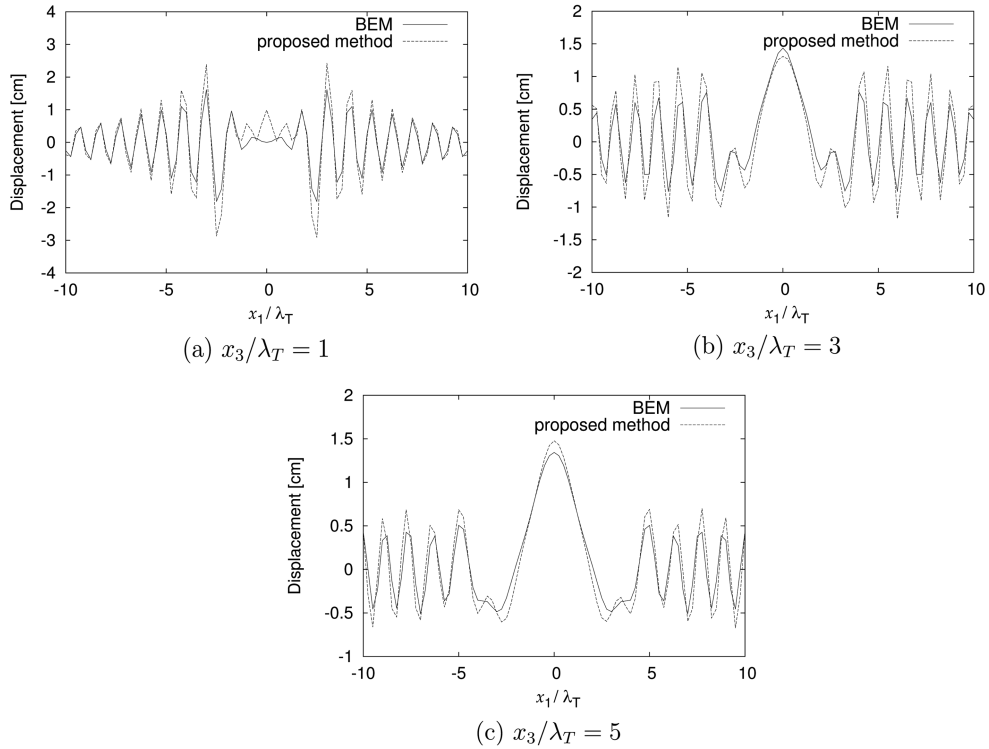


(a) boundary element method          (b) proposed method
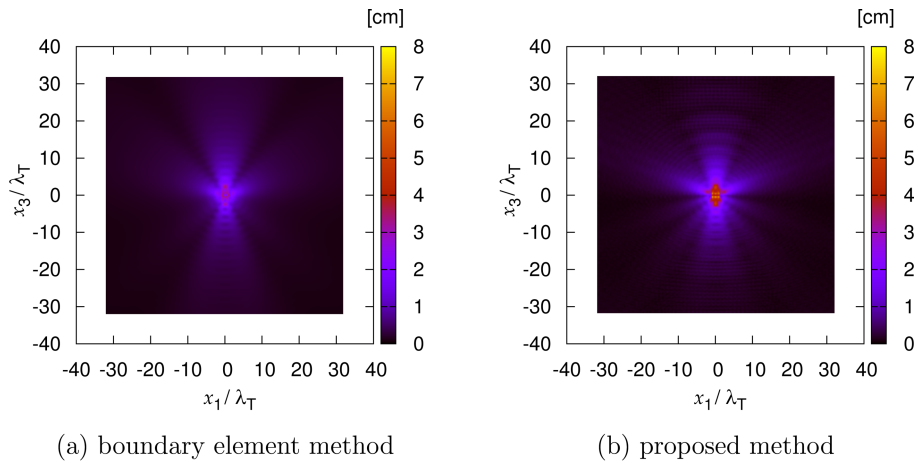
Fig. 7 Comparison of displacement amplitudes in the $x_1 - x_3$ plane

Fig. 6 compares the results obtained using the proposed method and the boundary element method. The real parts of the scattered waves along the $x_1$ axis are compared at the locations of $x_3/\lambda_T = 1$, 3 and 5. In Fig. 6, the $x_1$ axis is expressed in dimensionless form as $x_1/\lambda_T$. The present solution is obtained by the iterative process when the relative error becomes less than $\varepsilon_r = 0.001$ for the first

time. According to Fig. 6, the results show good agreement, which ensures the validity of constructing $\tilde{\delta}_\Gamma$ and the operator shown in Eq. (75) in the discrete Fourier transform. According to Fig. 6, the wavelength of the waves in the area of $|x_1/\lambda_T| \geq 5$ is found to be approximately equal to $\lambda_T$. This indicates that the $S$ wave is caused by the interaction between the inclusion and the plain incident $P$ wave.

Fig. 7 shows the amplitudes of the scattered waves in the $x_1 - x_3$ plane. For comparison, the results obtained from the boundary element method are also presented. Fig. 7 indicates that the directionality and the patterns of the scattered waves obtained using these methods are similar. The amplitude of the scattered waves in the area near the inclusion obtained by the proposed method, however, is found to be higher compared to the results obtained by the boundary element method. This corresponds to the results shown in Fig. 6(a). Therefore, the proposed method provides a higher displacement amplitude in the area near the rigid inclusion.

### 3.2 Scattering analysis of a cavity inclusion

The following example is a scattering analysis of a cavity inclusion embedded in a homogeneous elastic wave field. For this case, we solve Eq. (73) for the operator

$$\mathscr{A}_{Dij} = -\hat{\sigma}_{ikj}(\xi)\,\mathscr{F}_D\,(2\,\tilde{\delta}_I(x))n_k(x)\,\mathscr{F}_D^{-1} \tag{81}$$

The property of the material, the interval of grid points, the frequency of the analysis, and the incident wave field are the same as in the previous example.

The convergence of the solution for Eq. (73) by means of the Bi-CGSTAB method is shown in Fig. 8. In this case, the relative error is found to decrease rapidly compared to the case of the rigid inclusion shown in Fig. 5. Fig. 9 shows the comparison of the displacement of the real part of the scattered waves along the $x_1$ axis. As in the previous numerical example, the present solution is also obtained through an iterative process when the relative error of solutions becomes less than $\varepsilon_r = 0.001$ for the first time. The solutions obtained by the proposed method and by the boundary element method are compared. As shown in Fig. 9, good agreement of the solutions can be observed,
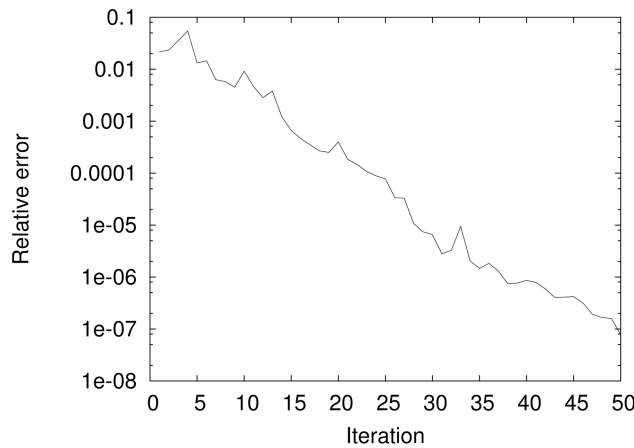


Fig. 8 Convergence properties of the solution

(a) $x_3/\lambda_T = 1$

(b) $x_3/\lambda_T = 3$

(c) $x_3/\lambda_T = 5$

Fig. 9 Comparison of displacement along the $x_1$ axis



(a) boundary element method

(b) proposed method
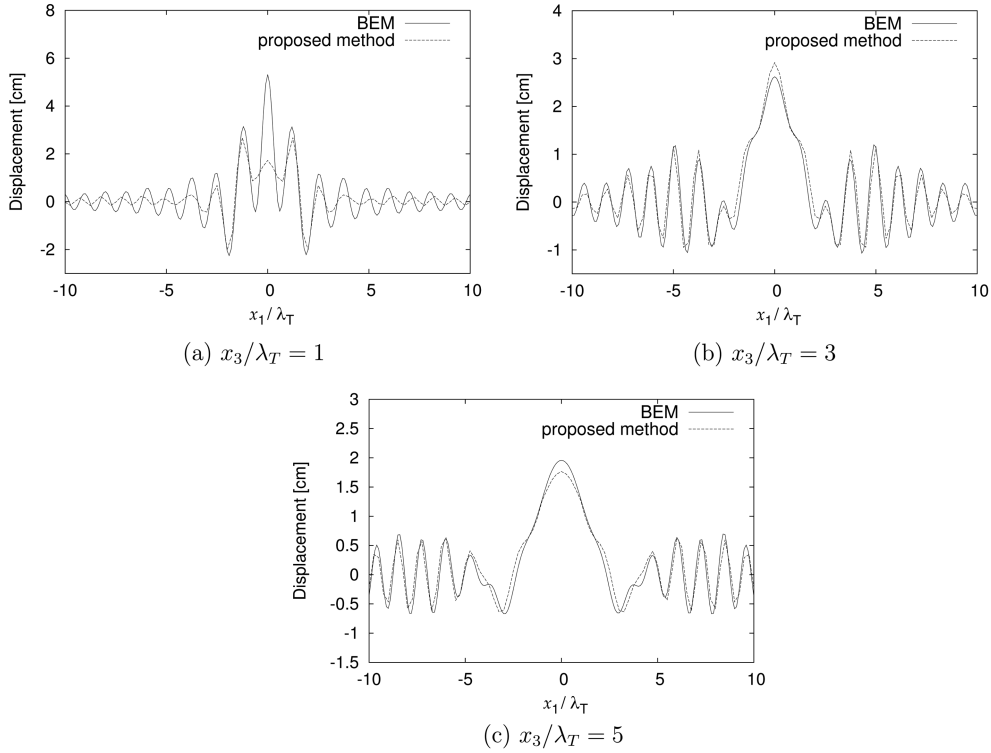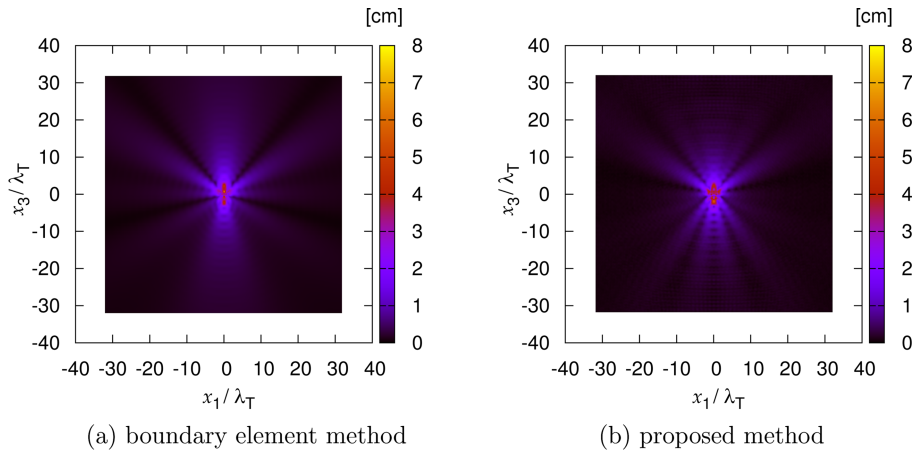
Fig. 10 Comparison of displacement amplitudes in the $x_1 - x_3$ planes

except in the case of $x_3/\lambda_T = 1$. In the case of $x_3/\lambda_T = 1$, the scattered waves are in the area near the inclusion. The displacement amplitude obtained using the boundary element method is much higher than that obtained using the proposed method around $x_1/\lambda_T \sim 0$. Except for this discrepancy, the displacement amplitudes for both methods are similar in this case. Fig. 9(b) and (c) indicate that the short wavelength of the scattered waves approximately equal to $\lambda_T$ can be observed as $x_1/\lambda_T$

becomes larger, as shown in Fig. 6. This indicates that $S$ wave propagation is caused by the interaction between the cavity inclusion and the plane incident $P$ wave.

Fig. 10 shows the amplitudes of the scattered waves in the $x_1 - x_3$ plane. For comparison, the results of the boundary element method are also presented. According to Fig. 10, the directionalities of the scattered waves are similar. In the area near the inclusion, however, the area of the high displacement amplitude is wider for the proposed method than for the boundary element method. A significant discrepancy with respect to the amplitudes of these methods, however, does not appear in Fig. 10.

### 3.3 Scattering analysis due to the interaction between a small cavity and fluctuations

The final numerical example is an analysis of scattered waves due to the interaction between a small cavity and fluctuations. The problem involves the solution of Eq. (73) with the operator

$$\mathscr{A}_{Dij} = \hat{h}_{ik}(\xi)\mathscr{F}_D N_{kj}(\partial, x)\mathscr{F}_D^{-1}$$
$$-\hat{\sigma}_{ikj}(\xi)\mathscr{F}_D (2\tilde{\delta}_I(x))n_k(x)\mathscr{F}_D^{-1} \tag{82}$$

The locations of the fluctuation and the cavity are shown in Fig. 11. The region for the fluctuation and the cavity is represented by a cube with sides of length equal to the wavelength of the $S$ wave. In addition, the fluctuation is expressed by

$$\tilde{\lambda}(x) = A_\lambda \chi_Q(x)$$
$$\tilde{\mu}(x) = A_\mu \chi_Q(x) \tag{83}$$

where $Q$ is the region for the fluctuation, and $A_\lambda$ and $A_\mu$ are the amplitude of the fluctuation that is set
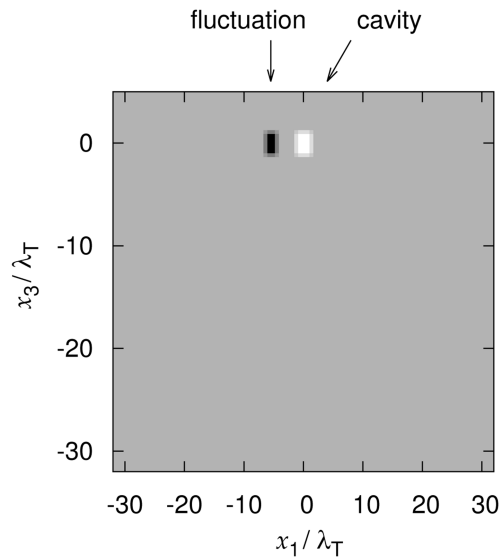


Fig. 11 Fluctuation and cavity in the wave field
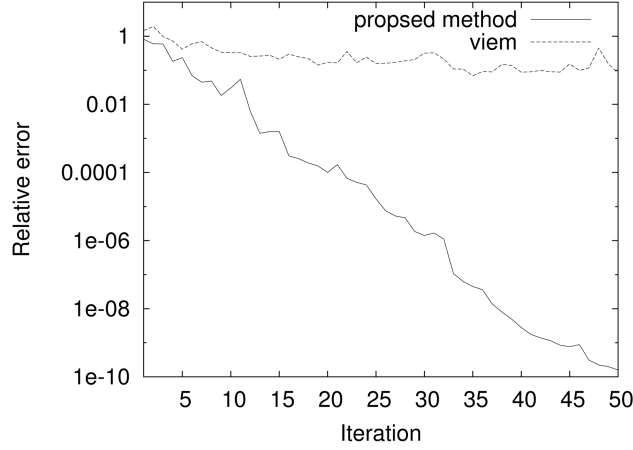
Fig. 12 Convergence properties of the solution

to $A_\lambda = A_\mu = 1$[GPa] for the numerical calculation. The derivatives of $\tilde{\lambda}$ and $\tilde{\mu}$, which are necessary to constitute $N_{jk}(\partial, x)$ shown in Eq. (82), are approximated by $A_\lambda/\Delta x_j$ and $A_\mu/\Delta x_j$, $(j = 1,2,3)$, respectively. These values are imposed on the interface boundary of the fluctuation. The number of grid points and the interval of grid points are $256 \times 256 \times 256$ and $\Delta x_j = 0.25$ km, respectively. In addition, the background structure of the wave field and the incident wave are the same as in the previous example.

The convergence properties of the solution obtained by the iterative Bi-CGSTAB method are shown in Fig. 12. For comparison, the convergence properties of the solution obtained by means of the following operator

$$\mathscr{A}_{Dij} = \hat{h}_{ik}(\xi)\,\mathscr{F}_D\,N_{kj}\,\mathscr{F}_D^{-1} \tag{84}$$

are also shown. In Fig. 12, the solution based on Eq. (84) is denoted by "viem", because the method is the volume integral equation method presented in the article by Touhei *et al.* (2009). For the analysis using the volume integral equation, the cavity is expressed by the fluctuation of the Lamé constants by setting

$$\tilde{\lambda}(x) = -\lambda_0$$
$$\tilde{\mu}(x) = -\mu_0, \quad x \in \Omega_i \tag{85}$$

and $\delta_\Gamma$ is excluded from the operator.

Fig. 12 shows that the relative error obtained using the proposed method decreases rapidly as the number of iterations increases. On the other hand, the relative error obtained from "viem" does not decrease even as the number of iterations increases. Therefore, the analysis of scattered waves by means of the operator shown Eq. (84) has a limitation. In order to improve the convergence properties of the volume integral equation method (Touhei *et al.* 2009), the introduction of $\delta_\Gamma$ into the operator is found to be important.

Fig. 13 shows the amplitudes of the scattered waves in the $x_1 - x_3$ plane. The amplitudes of the scattered waves from a cavity are found to be stronger than those from a fluctuating area, in which

the strong scattered waves are observed at the corner of the cubes. For this numerical example, the amplitudes of the fluctuations are not sufficient to cause strong scattered waves, compared to those from the cavity. Due to the directionality of the scattered waves, the interference of the scattered waves can also be observed on the forward side of the cavity and the fluctuation.

Fig. 14 shows the amplitudes of the scattered waves in the $x_1 - x_2$ plane on the forward side. The results are presented at the locations of $x_3/\lambda_T = 1$ and 2. According to Fig. 14(a), scattered waves can be observed just above the area of the fluctuation and the cavity. As shown in Fig. 13, the amplitude of the scattered waves from the cavity is higher than that from the fluctuating area. The directionality of the scattered waves from the cavity is found to be due to the waves generated at the corner. Figa. 14(a) and (b) indicate that the amplitude of the scattered waves decreases and the high-amplitude area spreads toward the far field. These results are reasonable and well explain the scattering phenomena.

At the end of this section, the CPU time required for scattering analysis is discussed. The processor
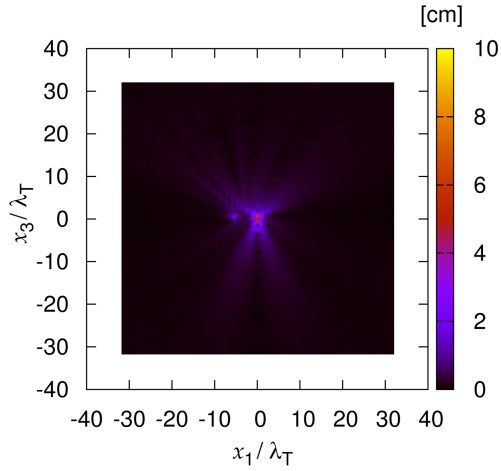


Fig. 13 Comparison of displacement amplitudes in the $x_1 - x_3$ plane



(a) $x_3/\lambda_T = 1$                    (b) $x_3/\lambda_T = 3$
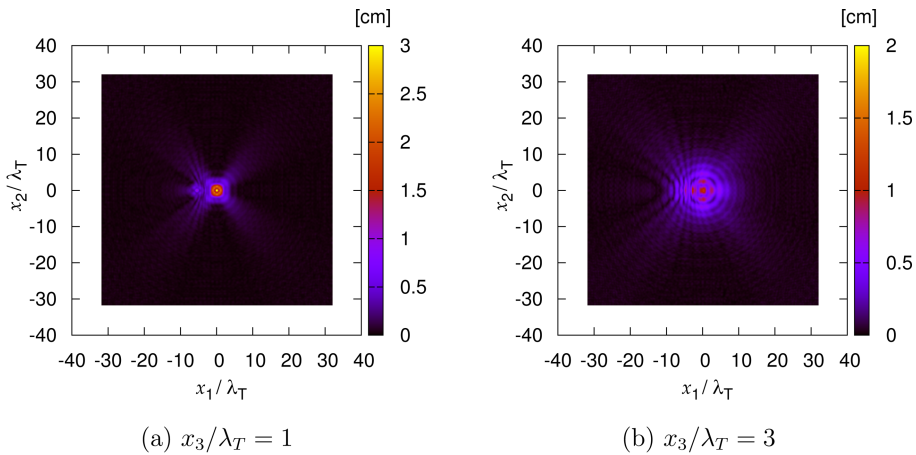
Fig. 14 Scattered waves in the $x_1 - x_2$ plane

used for the computation was an AMD Opteron 2387 processor. The ACML library was used for the fast Fourier transform. The number of iterations for a relative error of less than $1.0 \times 10^3$ was 16, and the CPU time was 38 minutes for this case. As mentioned earlier, the grid was a $256 \times 256 \times 256$ point grid. The CPU time consumption was primarily due to the fast Fourier transform for the 3D grid point model.

## 4. Conclusions

A coupled boundary-volume integral equation method was developed in order to analyze the scattering of elastic waves. The proposed method used the formulation in the wavenumber domain, in which the FFT is used to construct the Krylov subspace. The proposed method is an extension of the volume integral equation method, to which the effects of the boundary integral equation were introduced. The formulation of the proposed method focused primarily on transforming the boundary-volume integral equation into the volume integral equation in the wavenumber domain. The use of function $\delta_\Gamma$ was important in transforming the boundary-volume integral equation into the volume integral equation during the discrete Fourier transform. Therefore, a method for constructing $\tilde{\delta}_\Gamma$ and its numerical treatment were also clarified in the formulation. Numerical calculations were carried out to verify the formulation for the boundary-volume integral equation. According to the numerical results, the transform of the boundary-volume integral equation to the volume integral equation was successful. The present numerical results were found to be in good agreement with the results of the standard boundary element method. Furthermore, the convergence property of the solution due to the volume integral equation method (Touhei *et al*. 2009) is improved by the introduction of the effects of the boundary integral by means of $\delta_\Gamma$.

## References

Aki, K. and Richards, P.G. (2002), *Quantitative seismology*, 2nd Ed., U.S.A. University science books.
Barrett, R., Berry, M., Chan, T.F., Demmel, J., Donato, J.M., Dongarra, J., Eijkhout, V., Pozo, R., Romine, C. and Van der Vorst, H. (1994), *Templates for the solution of linear systems: building blocks for iterative methods*, SIAM.
Brebbia, C.A. and Walker, S. (1980), *Boundary element techniques in engineering*, London, Newness-Butterworth.
Colton, D. and Kress, R. (1983), *Integral equation methods in scattering theory*, New York, John Wiley & Sons, Inc.
Colton, D. and Kress, R. (1998), *Inverse acoustic and electromagnetic scattering theory*, Berlin, Springer.
De Zaeytijd, J., Bogaert, I. and Franchois, A. (2008), "An efficient hybrid MLFMA-FFT solver for the volume integral equation in case of sparse 3D inhomogeneous dielectric scatterers", *J. Comput. Phys*., **227**(14), 7052-7068.
Guzina, B.B., Fata, S.N. and Bonnet, M. (2003), "On the stress-wave imaging of cavities in a semi-infinite solid", *Int. J. Solids Struct*., **40**(6), 1505-1523.
Ikebe, T. (1960), "Eigenfunction expansion associated with the schroedinger operators and their applications to scattering theory", *Arch. Ration. Mech. Anal*., **5**(1), 1-34.
Manolis, G.D., Dineva, P.S. and Rangelov, T.V. (2004), "Wave scattering by cracks in inhomogeneous continua using BIEM", *Int. J. Solids Struct*., **41**(14), 3905-3927.
Markoe, A. (2006), *Analytic tomography*, New York, Cambridge University Press.
Touhei, T. (2009), "Generalized fourier transform and its application to the volume integral equation for elastic

wave propagation in a half space", *Int. J. Solids Struct*., **46**(1), 52-73.

Touhei, T., Kiuchi, T. and Iwasaki, K. (2009), "A fast volume integral equation method for the direct/inverse problem in elastic wave scattering phenomena", *Int. J. Solids Struct.*, **46**(21), 3860-3872.

Touhei, T. (2011), "A fast method for the volume integral equation for elastic wave propagation in a half space", *Int. J. Solids Struct*., **48**, 3194-3208.

Yang, J., Abubaker, A., van den Berg, P.M., Habashy, T.M., and Reitich, F. (2008), "A CG-FFT approach to the solution of a stress-velocity formulation of three-dimensional scattering problems", *J. Comput. Phys*. **227**(24), 10018-10039.